Journal of
Applied Crystallography
ISSN 0021-8898
Editor: **Anke R. Pyzalla**

Preferred orientation of ettringite in concrete fractures

Hans-Rudolf Wenk, Paulo J. M. Monteiro, Martin Kunz, Kai Chen, Nobumichi Tamura, Luca Lutterotti and John Del Arroz

J. Appl. Cryst. (2009). **42**, 429–432

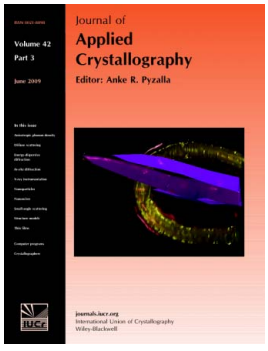

Journal of
Applied Crystallography
ISSN 0021-8898

Received 22 April 2009
Accepted 24 April 2009

Preferred orientation of ettringite in concrete fractures

Hans-Rudolf Wenk,[a]* Paulo J. M. Monteiro,[b] Martin Kunz,[c] Kai Chen,[c] Nobumichi Tamura,[c] Luca Lutterotti[d] and John Del Arroz[a]

[a]Department of Earth and Planetary Science, University of California, Berkeley, CA 94720, USA, [b]Department of Civil and Environmental Engineering, University of California, Berkeley, CA 94720, USA, [c]Advanced Light Source, Lawrence Berkeley Laboratory, 1 Cyclotron Road, Berkeley, CA 94720, USA, and [d]Department of Materials Engineering, University of Trento, 38050 Trento, Italy. Correspondence e-mail: wenk@berkeley.edu

Sulfate attack and the accompanying crystallization of fibrous ettringite [$Ca_6Al_2(OH)_{12}(SO_4)_3{\cdot}26H_2O$] cause cracking and loss of strength in concrete structures. Hard synchrotron X-ray microdiffraction is used to quantify the orientation distribution of ettringite crystals. Diffraction images are analyzed using the Rietveld method to obtain information on textures. The analysis reveals that the *c* axes of the trigonal crystallites are preferentially oriented perpendicular to the fracture surfaces. By averaging single-crystal elastic properties over the orientation distribution, it is possible to estimate the elastic anisotropy of ettringite aggregates.

1. Introduction

Preferred orientation has considerable influence on the properties of a wide range of materials. Microtextures have traditionally been measured using backscatter electron diffraction (*e.g.* Dingley, 2004), but this technique fails if crystallites are strained and contain large numbers of defects. In this case a focused X-ray beam can be employed as it is available at synchrotron sources. Early applications of synchrotron X-rays for texture analysis have been to thin films (Player *et al.*, 1992), plated alloys (Bäckstrøm *et al.*, 1996) and bone (Heidelbach *et al.*, 1999). Since then the technique has been greatly improved, especially by analyzing two-dimensional images using the Rietveld method (Lonardelli *et al.*, 2005). Here, we apply the technique to a different material, microscopic veins in deteriorating concrete that are filled with the mineral ettringite.

Concrete may be subject to sulfate attack that can cause expansion in the concrete matrix and lead to loss of strength and stiffness because of a lack of cohesiveness in the cement hydration products. The source of sulfate ions can be external or internal. For external sulfate attack, sulfate in groundwaters can penetrate the porous concrete matrix and react with hydration products, leading to expansion and cracking of the matrix. There is a consensus that this expansion in concrete is caused by the crystallization of ettringite, $Ca_6Al_2(OH)_{12}(SO_4)_3{\cdot}26H_2O$, formed from the monosulfate hydrate $Ca_4Al_2(OH)_{12}(SO_4){\cdot}6H_2O$ which is present in the cement paste (*e.g.* Mehta & Monteiro, 2006). Other phases, such as $Ca_4Al_2O_{26}H_{38}$, $Ca_3Al_2O_6$ and $Ca_4Al_2Fe_2O_{10}$, can also be sources of aluminate ions in the formation of ettringite. The reaction to generate ettringite from the monosulfate starts with the dissolution of the latter, according to

$$Ca_4Al_2(OH)_{12}(SO_4){\cdot}6H_2O \rightarrow 4Ca^{2+} + 2Al(OH)_4^- + 4OH^- + SO_4^{2-} + 6H_2O, \quad (1)$$

which leads to the precipitation of ettringite during external sulfate attack,

$$6Ca^{2+} + 2Al(OH)_4^- + 4OH^- + 3SO_4^{2-} + 26H_2O \rightarrow Ca_6Al_2(OH)_{12}(SO_4)_3{\cdot}26H_2O. \quad (2)$$

Equation (2) indicates that a source of Ca^{2+} ions is also necessary for the growth of ettringite. In the cement paste, calcium hydroxide, $Ca(OH)_2$ (portlandite), is the first phase to dissolve, according to

$$Ca(OH)_2 \rightarrow Ca^{2+} + 2OH^-. \quad (3)$$

Once calcium hydroxide is no longer available, calcium silicate hydrates start to dissolve. Since calcium silicate hydrates are the continuous phase in the cement paste responsible for its strength and stiffness, the decalcification of these silicates leads to a deterioration in mechanical properties.

In the case of internal sulfate attack, the sources of sulfate ions are internal, for instance when aggregates contaminated with gypsum are used in the concrete manufacture. Delayed ettringite formation (DEF) is a special case of internal sulfate attack where concrete structures, exposed to high temperature during curing, can suffer expansion and cracking after a few years in operation. The typical manifestation of distress is the presence of voids around the coarse aggregate, indicating expansion of the cement paste. Often these voids are filled with ettringite crystals, which also fill other voids and cracks in

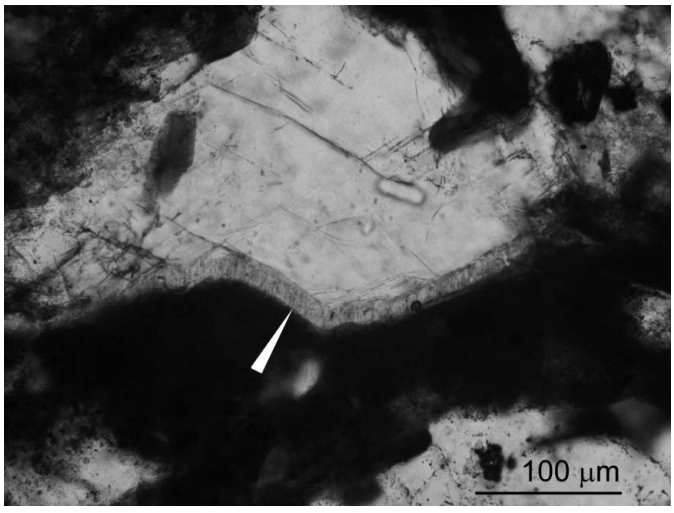

Figure 1
Optical micrograph of a thin section of concrete with cement paste (dark) and a large feldspar aggregate fragment (transparent). At the interface is a vein of fibrous ettringite (arrow).

the matrix. Although there is no consensus on the mechanism of expansion caused by DEF, there is a general agreement that ettringite is not a product of cement hydration when concrete is cured at temperatures exceeding 343 K. Instead, calcium monosulfoaluminate is formed, with much of the sulfate adsorbed in the calcium silicate hydrates. Later, during service, when sulfate ions are desorbed, calcium monosulfoaluminate is transformed into ettringite, which, on exposure to high humidity, causes expansion and microcracking in the matrix and generates a gap around the aggregate (Taylor, 1997). With time and in the presence of moisture, large crystals of ettringite develop from smaller ones and fill the gap.

2. Samples and texture analysis

Samples were collected from a building in Recife, Brazil. The concrete foundations showed a significant amount of distress. The reason for the expansive reaction was originally attributed to the alkali–silica reaction (ASR), which involves certain siliceous aggregates and a highly alkaline concrete pore solution reacting to produce an expansive alkali–silicate gel, which can imbibe water and then expand. Many dams, pavements and reinforced concrete bridges require continuous repair or replacement because of cracks caused by this deleterious reaction. Field studies of damaged concrete structures have documented that the distress can be caused by both ASR and DEF (Johansen *et al.*, 1993; Pettifer & Nixon, 1980; Shayan & Quick, 1992).

A sample of such deteriorating concrete shows conspicuous fractures filled with a fibrous material when viewed with a petrographic microscope (Fig. 1). The veins are about 10–20 μm wide and composed of calcium, aluminium and sulfur, as established by electron microprobe analyses.

We decided to use the microfocus beamline 12.3.2 at the Advanced Light Source (ALS) of the Lawrence Berkeley National Laboratory (LBNL) for phase identification by diffraction and for determination of preferred orientation. This beamline is mainly used to quantify residual lattice strains from single-crystal Laue patterns (Tamura *et al.*, 2003). A first series of experiments with white radiation was unsuccessful because the Laue patterns displayed extreme asterism. We then changed strategy and used monochromatic radiation in transmission. We have previously performed similar experiments with hard X-rays at the APS (11-ID-C) and the ESRF (ID-15B) (*e.g.* Wenk *et al.*, 2006, 2008), but at those beamlines the beam size is much larger than the dimensions of the ettringite vein. Microfocus beamline ID-11 at the ESRF would also be suitable for similar experiments.

Sample preparation is delicate because standard petrographic thin sections cannot be applied to this material, which is sensitive to heat, air and moisture. A flat surface was impregnated with epoxy resin and then mounted on a glass slide using Superglue. Using a diamond saw, and with kerosene as cooling agent, a thin slice was prepared, which was then ground to 50 μm and also sealed with epoxy. Finally, the slice was removed from the glass slide and used for the investigation. Interesting areas were identified with a light microscope and marked (Fig. 1). Subsequently, the sample was mounted on a translating goniometer on beamline 12.3.2 with a MarResearch 133 CCD detector, more or less centered on the incident X-ray behind the sample. Images were collected between 30 and 60 s. The wavelength was 1.5498 Å (8 keV). The sample-to-detector distance was calibrated with a corundum (alumina) powder.

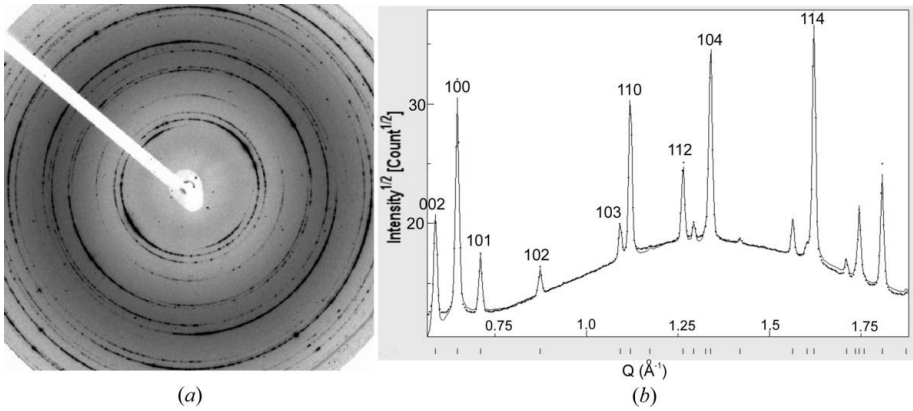

Figure 2
(*a*) Diffraction image of polycrystalline ettringite. Intensity variations around the Debye rings are indicative of preferred orientation. (*b*) Diffraction pattern obtained by azimuthal average. Crosses are experimental data and the line is the Rietveld fit.

Diffraction images with a 2 × 2 μm beam immediately reveal a polycrystalline pattern with Debye rings that can be indexed as ettringite (Fig. 2). There are azimuthal intensity variations indicative of preferred orientation. Qualitatively, the *c* axis of

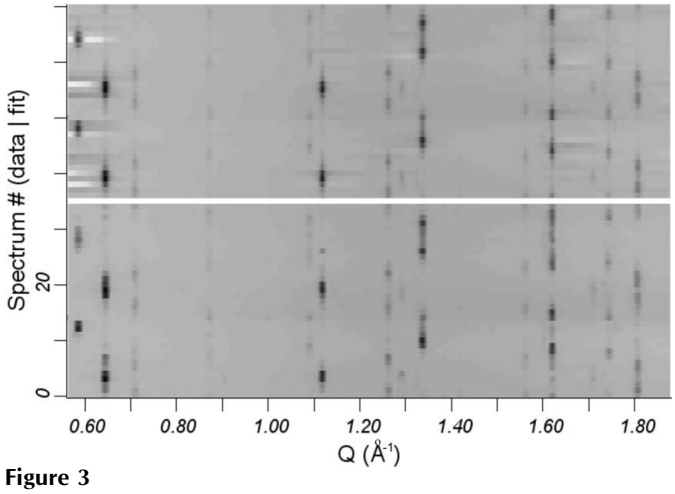

Figure 3
Two-dimensional representation of a stack of 36 diffraction spectra as a function of azimuth (vertical axis) and diffraction angle transformed to $Q = 2\pi/d$ (horizontal axis). At the bottom are observations and at the top the Rietveld fit. The pattern displays a strong texture and an excellent fit.

this trigonal mineral can be associated with the fiber direction. The images were then further processed in *Fit2D* (Hammersley, 1998) to correct for detector distance and detector orientation, and to extract integrated diffraction spectra over 10° azimuthal intervals. These spectra were then used for a Rietveld refinement with the program *MAUD* (Version 2.073; Lutterotti *et al.*, 1997, 2004). The program refines, in cycles, background and instrumental parameters, crystallographic parameters and texture. As a starting structure we used ettringite as refined by Goetz-Neunhoeffer & Neubauer (2006) (space group *P*31*c*), which is similar to the structure reported by Hartman & Berliner (2006). The crystal structure was not refined, as the range and resolution were not sufficient for a full Rietveld refinement and the structural intensities reproduced sufficiently the published structures. The texture was refined by two methods: using *E-WIMV* (Matthies & Vinel, 1982), assuming axial symmetry, and by refining a standard Gauss function with cylindrical symmetry. Both methods provide similar results. Fig. 2(*b*) shows the average spectrum, which illustrates a good fit with ettringite, and Fig. 3 compares a two-dimensional plot of stacked observed spectra with recalculated spectra and documents a good fit for intensity variations with azimuth. The final R_{wp} indices of the refinement were around 0.15 for both texture models and this is a good value considering a strong texture. The orientation distribution was then exported and used in *BEARTEX* (Wenk *et al.*, 1997) to calculate and plot pole figures and inverse pole figures.

3. Results

Pole figures view the sample perpendicular to the fracture surface. They display a strong maximum of *c* axes perpendicular to the fracture surface (Fig. 4*a*) and, correspondingly, *a* axes distributed in a girdle parallel to the fracture surface (Fig. 4*b*). The *c*-axis texture maximum is 28 multiples of a random distribution (m.r.d.). This is a very strong alignment

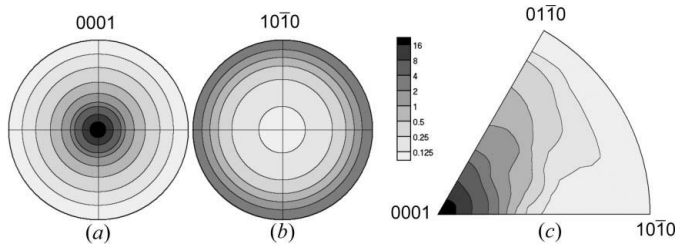

Figure 4
(*a*) and (*b*) Pole figures and (*c*) inverse pole figure of the fiber axis, illustrating the preferred orientation of ettringite. Equal area projection. Logarithmic contours are in multiples of a random distribution.

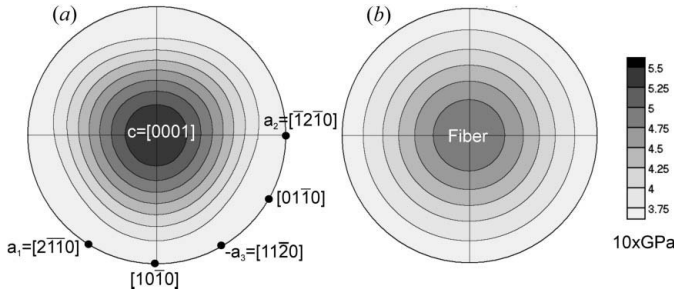

Figure 5
Elastic longitudinal stiffness surfaces for (*a*) a trigonal ettringite single crystal in crystal coordinates and (*b*) a vein aggregate projected on the fracture surface.

with a peak width at half-maximum of less than 10° for the *E-WIMV* analysis and 10.4° for the standard function. Axially symmetric textures are conveniently represented in inverse pole figures (Fig. 4*c*). The plot confirms that the texture is basically produced by a *c*-axis alignment with no further constraints. We investigated several spots along the ettringite vein and found minor variations, with local texture strengths varying between 15 and 30 m.r.d.

4. Discussion and conclusions

A focused synchrotron X-ray beam proved to be an ideal method to investigate crystallite orientations in 10–20 µm-thick veins of ettringite in concrete, and the microfocus beamline at ALS has proved to be a powerful tool for investigating the preferred orientation of crystallites in very small volumes of poorly crystalline air- and heat-sensitive materials. By analyzing a thin slab, protected with epoxy coatings, in transmission, areas as small as 2 × 2 µm could be selected for analysis with an X-ray energy of 8 keV. The two-dimensional diffraction images could be processed using the Rietveld method, even though there is considerable spottiness (Fig. 2*a*) due to limited grain statistics.

In the case of this concrete sample, the orientation of the ettringite crystals is highly significant for the strength of the material. In ettringite, the *c* axis is the elastically stiffest direction (Speziale, Jiang *et al.*, 2008), contrary to the cement mineral portlandite [$Ca(OH)_2$], which also shows preferred orientation in veins (Detwiler *et al.*, 1988) and where the *c* axis is elastically softest (Speziale, Reichmann *et al.*, 2008). The

single-crystal elastic tensor of trigonal ettringite (C_{11} = 35.1, C_{12} = 21.9, C_{13} = 20.0, C_{14} = 0.6, C_{33} = 55.0 and C_{44} = 11.0 GPa) was averaged over the orientation distribution, using the geometric mean method (Matthies & Humbert, 1993), providing stiffness coefficients C_{11} = 36.3, C_{12} = 21.7, C_{13} = 20.5, C_{14} = 0.0, C_{33} = 49.7 and C_{44} = 10.6 GPa, assuming axial symmetry. Fig. 5 compares the longitudinal stiffness surfaces for an ettringite single crystal (*a*) with that for the vein aggregate (*b*). The anisotropy [An = 200(max − min)/(max + min)%] is 44% for the single crystal and 31% for the ettringite aggregate.

We acknowledge access to beamline 12.3.2 at the ALS of the LBNL and discussions with Sergio Speziale (Potsdam). This publication was based on work supported in part by award No. KUS-I1-004-21 made by the King Abdullah University of Science and Technology (KAUST) (to PJMM and HRW) and by NSF grant No. EAR 0836402. The ALS is supported by the Director, Office of Science, Office of Basic Energy Sciences, Materials Sciences Division of the US Department of Energy under contract No. DE-AC02-05CH11231 at the LBNL.

References

Bäckstrøm, S. P., Riekel, C., Abel, S., Lehr, H. & Wenk, H. R. (1996). *J. Appl. Cryst.* **29**, 118–124.
Detwiler, R. J., Monteiro, P. J. M., Wenk, H.-R. & Zhong, Z. (1988). *Cem. Concr. Res.* **18**, 823–829.
Dingley, D. (2004). *J. Microsc.* **213**, 214–224.
Goetz-Neunhoeffer, F. & Neubauer, J. (2006). *Powder Diffract.* **21**, 4–11.
Hammersley, A. P. (1998). *Fit2D, V99.129 Reference Manual Version 3.1*. Internal Report ESRF-98-HA01, ESRF, Grenoble, France.
Hartman, M. R. & Berliner, R. (2006). *Cem. Concr. Res.* **36**, 364–370.
Heidelbach, F., Riekel, C. & Wenk, H.-R. (1999). *J. Appl. Cryst.* **32**, 841–849.
Johansen, V., Thaulow, N. & Skalny, J. (1993). *Adv. Cem. Res.* **5**, 23–29.
Lonardelli, I., Wenk, H.-R., Lutterotti, L. & Goodwin, M. (2005). *J. Synchrotron Rad.* **12**, 354–360.
Lutterotti, L., Chateigner, D., Ferrari, S. & Ricote, J. (2004). *Thin Solid Films*, **450**, 34–41.
Lutterotti, L., Matthies, S., Wenk, H.-R., Schultz, A. S. & Richardson, J. W. (1997). *J. Appl. Phys.* **81**, 594–600.
Matthies, S. & Humbert, M. (1993). *Phys. Status Solidi B*, **177**, K47–K50.
Matthies, S. & Vinel, G. W. (1982). *Phys. Status Solidi B*, **122**, K111–K114.
Mehta, P. K. & Monteiro, P. J. M. (2006). *Concrete. Microstructure, Properties, and Materials*, 3rd ed. New York: McGraw–Hill.
Pettifer, K. & Nixon, P. J. (1980). *Cem. Concr. Res.* **10**, 173–181.
Player, M. A., Marr, G. V., Gu, E., Savaloni, H., Öncan, N. & Munro, I. H. (1992). *J. Appl. Cryst.* **25**, 770–777.
Shayan, A. & Quick, G. W. (1992). *Am. Concr. Inst. Mater. J.* **89**, 348–361.
Speziale, S., Jiang, F., Mao, Z., Monteiro, P. J. M., Wenk, H.-R., Duffy, T. S. & Schilling, F. (2008). *Cem. Concr. Res.* **38**, 885–889.
Speziale, S., Reichmann, H. J., Schilling, F. R., Wenk, H. R. & Monteiro, P. J. M. (2008*b*). *Cem. Concr. Res.* **38**, 1148–1153.
Tamura, N., MacDowell, A. A., Spolenak, R., Valek, B. C., Bravman, J. C., Brown, W. L., Celestre, R. S., Padmore, H. A., Batterman, B. W. & Patel, J. R. (2003). *J. Synchrotron Rad.* **10**, 137–143.
Taylor, H. F. W. (1997). *Cement Chemistry*, 2nd ed. London: T. Telford.
Wenk, H.-R., Lonardelli, I., Rybacki, E., Dresen, G., Barton, N., Franz, H. & Gonzalez, G. (2006). *Phys. Chem. Miner.* **33**, 667–676.
Wenk, H.-R., Matthies, S., Donovan, J. & Chateigner, D. (1998). *J. Appl. Cryst.* **31**, 262–269.
Wenk, H.-R., Voltolini, M., Kern, H., Popp, H. & Mazurek, M. (2008). *Leading Edge*, **27**, 742–748.